Open Research Online

The Open University's repository of research publications
and other research outputs

A quantitative evolved gas analysis for extra-terrestrial samples

Journal Item

For guidance on citations see FAQs.

oro.open.ac.uk

Journal Pre-proof

A quantitative evolved gas analysis for extra-terrestrial samples

A.B. Verchovsky, M. Anand, S.J. Barber, S. Sheridan, G.H. Morgan

Please cite this article as: Verchovsky, A.B., Anand, M., Barber, S.J., Sheridan, S., Morgan, G.H., A quantitative evolved gas analysis for extra-terrestrial samples, *Planetary and Space Science* (2020), doi: https://doi.org/10.1016/j.pss.2019.104830.

1   **A QUANTITATIVE EVOLVED GAS ANALYSIS FOR EXTRA-TERRESTRIAL SAMPLES.**

2   A. B. Verchovsky, M. Anand, S. J. Barber, S. Sheridan and G. H. Morgan

3   School of Physical Sciences, The Open University, Milton Keynes, MK7 6AA (sasha.verchovsky@open.ac.uk)

4   Abstract

5   Evolved gas analysis (EGA) has been successfully applied to the studies of meteorites and Apollo lunar

6   samples. It consists of linear heating of a material with registration of the released volatile compounds, typically

7   using a spectrometric technique. However, so far no quantitative comparison was possible of the amount of

8   gases released during heating of a sample. To address this limitation, we have developed a Quantitative EGA

9   (QEGA) technique using our custom-built Finesse mass spectrometry system. It is based on calibration of the

10   quadrupole mass spectrometer with reference gases (e.g. CO_2, CO, H_2, O_2, N_2 or their mixtures with known

11   relative abundances) with known flow rate. The method was tested using simple chemical compounds such as

12   $CaCO_3$, which give well-known amounts of pure gases during their thermal decomposition. We present initial

13   QEGA data on two reference meteorites, Allende and Murchison. Our QEGA work is also informing the design

14   and operation of ProSPA spaceflight instruments being developed to perform analogous experiments *in situ* on

15   the lunar surface through the European Space Agency's PROSPECT payload on Luna 27.

16   Keywords: Evolved Gas Analysis; Volatiles; Meteorites; Allende; Murchison

21   **1. Introduction**

22   Evolved gas analysis (EGA) is a powerful tool widely used in different research applications from

23   investigations of chemical compounds in chemistry (polymers, complexes, catalysts, composite materials etc.)

24   and technology (coating, food production, batteries etc.) to environment and Earth Sciences (see Risoluti and

25   Materazzi, 2018 and references therein). It consists of linear heating of a material with registration of the

26   released volatile compounds by different methods such as gas chromatography, infrared spectroscopy and mass

27   spectrometry (MS). The latter seems to be the most universal and effective method of volatiles registration, and

28   if a quadrupole mass spectrometer (QMS) is used, it enables rapid identification of a wide range of evolved

29 gases through the characteristic mass-to-charge ratio (m/z) of their fragment ions. Often the EGA is used in

30 combination with thermoanalysis (TA) or thermogravimetric analysis (TGA). TA-MS EGA allows

31 identification of temperature effects during heating of materials as a result of their structural transformations

32 while TGA-MS EGA additionally records mass loss. Thus TGA-MS gives a possibility not only to identify

33 released gases, obtain their release patterns as a function of temperature and establish corresponding mass loss

34 but also to associate them with mechanisms of their release such as chemical reactions or structural

35 transformation occurring in the heated materials.

36 Investigations of gases in rocks have always been an important theme in geology starting from pioneering

37 works at the beginning of the twentieth century (Chamberlin, 1909) and continuing through to investigations of

38 Martian rocks by the Curiosity rover (Ming et al., 2014). EGA applied to Earth Sciences aims primarily to

39 identify gases trapped within rocks or minerals in order to characterise fluid environment during their formation

40 or later transformations such as metamorphism or metasomatism. An interesting application for terrestrial

41 samples is a combination of EGA with continuous crushing (Xiao et al., 2019), which allows separation of gases

42 trapped in fluid inclusions from those released from the lattice. For extra-terrestrial materials, especially in case

43 of lunar samples, the solar wind implanted gases are also of interest. EGA was successfully applied to Apollo

44 lunar samples in the early 1970s (Gibson et al., 1971, 1972). Gases from implanted solar wind (H_2, He) and

45 inclusions (CO, CO_2, N_2) together with gases (CO) released as a result of chemical reactions among minerals

46 have been identified. Different lunar samples can be compared with each other in terms of the release patterns of

47 different gas species. However, a quantitative comparison of the amount of gases present in different samples

48 has not been previously achieved. In these previous studies, it also was not possible to compare the relative

49 amounts of gases released by a single sample either, as often the release profile at each m/z ratio was normalised

50 to its maximal value.

51 This work, therefore, aims at developing Quantitative EGA (QEGA), in order to enable new insights into

52 laboratory analyses of extra-terrestrial samples. In addition, QEGA would inform the design and operation of

53 spaceflight instruments being developed to perform analogous experiments *in situ* on the lunar surface such as

54 within the European Space Agency's PROSPECT package (Barber et al., 2018). The quantitative determination

55 of volatiles within lunar regolith is also important for lunar *in situ* resource utilization (ISRU) (Anand et al.,

56 2012).

57 Several authors have previously reported on attempts to develop QEGA for TA-MS and TGA-MS systems

58 which use a carrier gas (Maciejewski and Baiker, 1997; Xia and Wei, 2015). This requires calibration of QMS

59   sensitivity for different gases and flow rate of the carrier gas. For calibration, pure gases as well as compounds

60   with well-known decomposition stoichiometry (e.g. $NaHCO_3$) were used.

61   In this study we developed a QEGA just for the QMS system without a carrier gas by calibration of the

62   measuring instrument with reference gases, for which the flow rate is determined independently, in order to

63   convert the signals from different gas species from samples into their flow rates, ultimately leading to their

64   quantification and allowing comparison with different samples. The method has been applied for analyses of

65   Murchison and Allende reference samples, prepared in the context of ESA's PROSPECT activity (Mortimer et

66   al., 2017).

67   2. **Experimental set up and measurement procedures**

68   The experimental setup is shown in Fig. 1. It is a part of our Finesse mass spectrometric system for multi-

69   element analyses (Verchovsky, 2017). Reference gas from a high-pressure (up to 200 bars) cylinder was placed

70   into pre-evacuated reference gas vessel (~0.5 l) via valves 1 and 2, at 4-10 bar pressure, as measured with a

71   mechanical pressure gauge. Valve 2 was kept open, to monitor the pressure stability throughout the calibration

72   process. The MKS Baratron® capacitance manometer provides a 10 volt output at its 1 torr upper limit with a

73   resolution of 0.01 mV thus giving 6 orders of magnitude dynamic range for flow rate measurements of reference

74   gases. The flow rate was regulated with a piezo-electrically actuated (lead zirconate titanate or 'PZT') metering

75   valve (Sheridan et al., 2010) which provides a variable flow restriction as a function of an applied regulating

76   voltage in the range 0-100 V. The PZT valve provides an analogous functionality to a standard capillary with

77   crimp (Sheridan et al., 2010), providing an acceptably stable flow rate at a given operating voltage (see sect.

78   3.1). The flow rate of a reference gas is determined by its accumulation in the volume between PZT valve and

79   Baratron® for a certain amount of time when valves 4, 7 and 12 are opened and valves 3, 5, 6, 8, 9 and 10 are

80   closed and the PZT valve is opened at a constant voltage. Then valve 4 is closed and the Baratron® pressure (in

81   mbar) is recorded after 20 second of gas equilibration time. Afterwards, the gas is pumped away with turbo and

82   ion pumps via valves 5 and 9, respectively and the procedure is repeated several times for different

83   accumulation time with unchanged PZT valve voltage. This procedure yields flow rate in mbar/s. In order to

84   express the flow rate in cc/s the volume from PZT valve to Baratron® was determined by putting helium in this

85   volume at a certain pressure (Po); after equilibration with the volume-calibrated container (Vc) the pressure P1

86   is recorded while V6 is opened. The volume where the gas was accumulated during flow rate determination is

87   found as:

88   P1*Vc/(Po-P1).
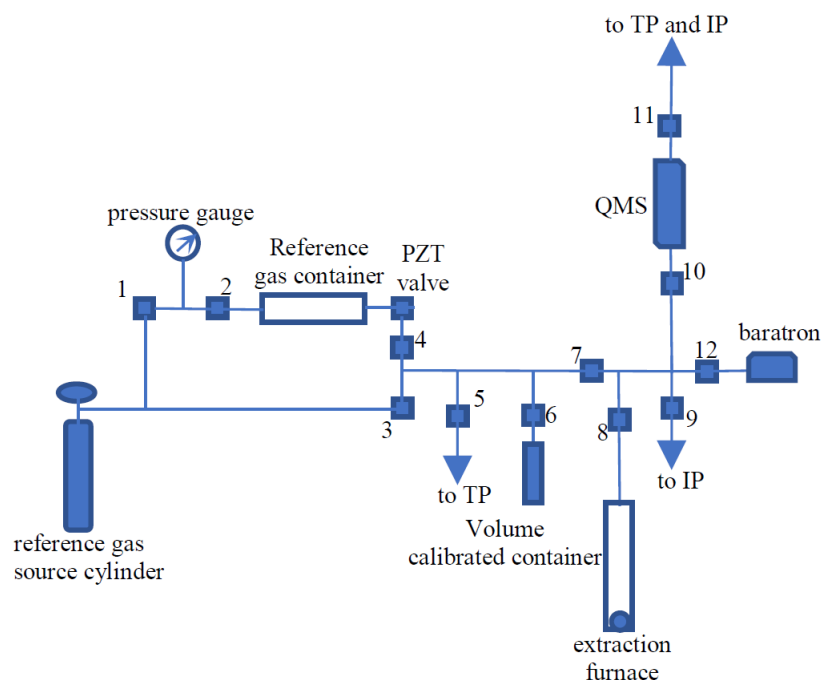

Figure 1. Schematic of the experimental setup

91   Directly after the flow rate calibration the reference gas was directed to the QMS via valves 4, 7 and 10 with

92   valves 3, 5, 6, 8, 9 and 12 closed keeping PZT voltage the same and the signals for a number of masses in the

93   range from 2 to 132 were recorded in the continuous flow pumping gas through QMS via valve 11 to turbo and

94   ion pumps working in parallel. The signals were registered using peak jumping mode and ion counting. For the

95   same reference gas, the procedure was repeated several times for different flow rates in the range from 10^{-8} to

96   10^{-4} mbar/s.

97   Following calibration, EGA was performed by putting a sample (wrapped in platinum foil) into the

98   extraction furnace and subjected to linear heating in the range from 100 to 1400 ^{o}C. The released gases were

99   continuously pumped through QMS via valves 8, 10 and 11 (with valves 7, 9 and 12 closed) with registration of

100   the same masses as during calibration. Additionally, blank experiments were performed using empty Pt foils.

101   During QMS measurements we monitored pressure measured by the ion pump controller. These

102   measurements are not particularly precise, nevertheless, correlation between the pressure and flow rate is

103   relatively good (Fig. 2). This gives us an opportunity to use this pressure as an independent indication of gas

104   release during sample analyses.

105 We note that the system was not particularly designed for water analysis, since the pipes between the

106 extraction furnace and QMS were not heated to 100 ^{o}C in order to prevent water condensation.

107 All the procedures described above, apart from filling the reference vessel with a reference gas, are fully

108 automated and controlled by a computer. All valves, except 1 and 2 are pneumatically activated, controlled by

109 solenoid valves, which in turn are controlled via optically isolated digital output NI1705 card. The Baratron

110 output was connected to a Keithley digital voltmeter, and as the voltage source for PZT valve, we used Keithley

111 6487 Picoammeter/Voltage source both controlled via serial ports.
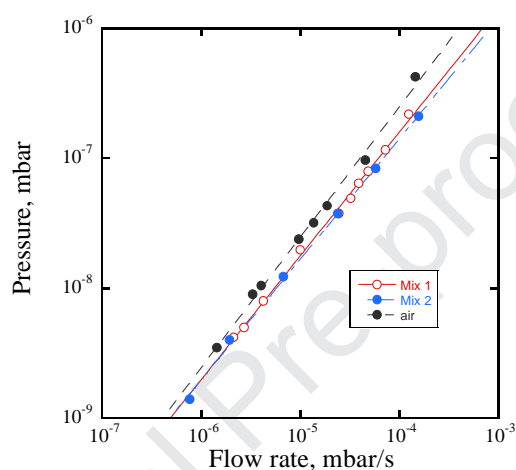
112

113 Figure 2. Correlation between flow rate and pressure measured on ion pump for different gas mixtures. Note that

114 the pressure measured by the ion pump is gas specific, for which reason the lines for different gas mixtures are

115 not coincident with each other.

116 3. **Results**

117 3.1. *Flow rate calibration*

118 For the flow rate calibration, we used pure gases such as CO_2, CO, O_2, H_2, N_2, CH_4, two artificial gas

119 mixtures, containing 11 common gases with the relative abundances (resembling those of lunar soils) shown in

120 Table 1 and a mixture with atmospheric composition. The mixtures were prepared by Air Products with

121 precision for relative abundances of the individual species better than 2 per cent and were stored into 50 L

122 cylinders with 200 and 12 bar pressure for Mixtures 1 and 2, respectively. A standard 200 L cylinder with

123 compressed air at 80 bar pressure was used as a reference gas mixture with atmospheric composition.

124 Table 1 Relative abundances (vol.%) of gases in the reference mixtures

5

gas	H$_2$	He	CH$_4$	Ne	N$_2$	CO	O$_2$	Ar	CO$_2$	Kr	Xe
Mixture 1	69.66	9.048	0.999	0.0997	10.027	1.001	0.020	0.02035	9.988	0.01991	0.01495
Mixture 2	56.78	15.91	1.452	0.1011	15.42	1.030	2.98	1.002	5.288	0.02022	0.01516

125

126   For this calibration, accumulation times from 10 to 100 s with 10-20 s increment were used. Typical

127   calibration lines are shown in Figure 3. The slopes of the lines give flow rate in mbar/s, that can be converted

128   into cc/s as stated above. Precision of the slopes is within 1-2% (1☐).
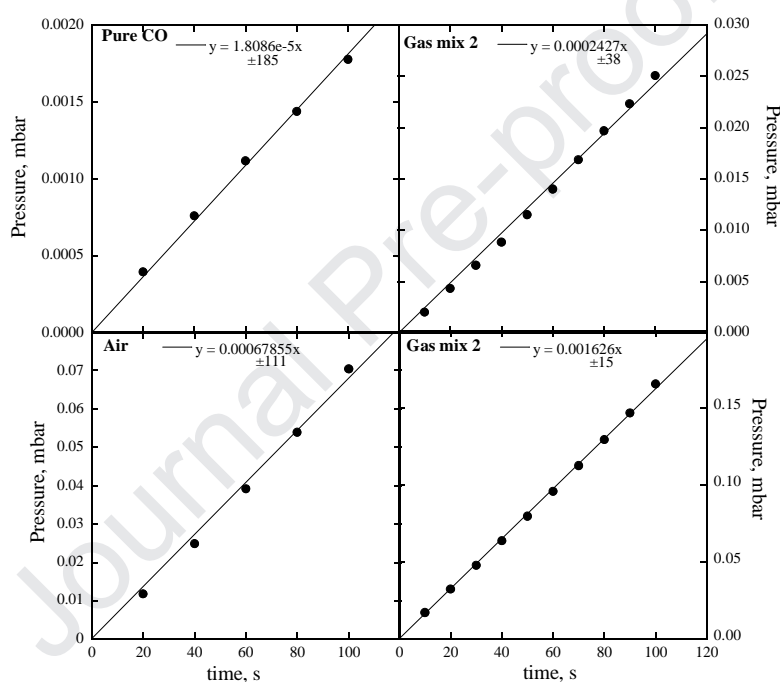
129

130   Figure 3. Examples of flow rate calibration. Errors on slopes are shown for the corresponding final two or

131   three digits.

132

133   3.2. *QMS sensitivity calibration*

134   During continuous pumping of a reference gas with known flow rate through QMS (after pressure is

135   stabilised) the intensities of 10-20 masses in the range from 2 to 132 (m/z=2, 3, 4, 12, 14, 16, 17, 18, 20, 22, 27,

136   28, 29, 30, 32, 36, 39, 40, 44, 84, 132) were recorded during 200 scans using peak jumping mode with 20 ms

137   integration time. The procedure was repeated 3 times with 5 min pumping time between measurements. The

138   dependence of peak intensities on flow rate represents QMS sensitivity with respect to different species. The

139   best fit for the experimental points in the wide range (several orders of magnitude) of QMS signals and flow

140   rates approximates to a power law (Fig. 4). The QMS sensitivity is expressed as cps/(mbar/s) or cps/(cc/s) and

141   depends on flow rate. It is important to note here that pure gases and gas mixture give indistinguishable

142   calibration curves over the range of a few orders of magnitude, indicating that no significant element

143   fractionation occurs during transition of a gas between the reference gas container and QMS, since flow rates of

144   individual gases in the gas mixtures were found using the relative abundances of the gases from the Table 1.

145
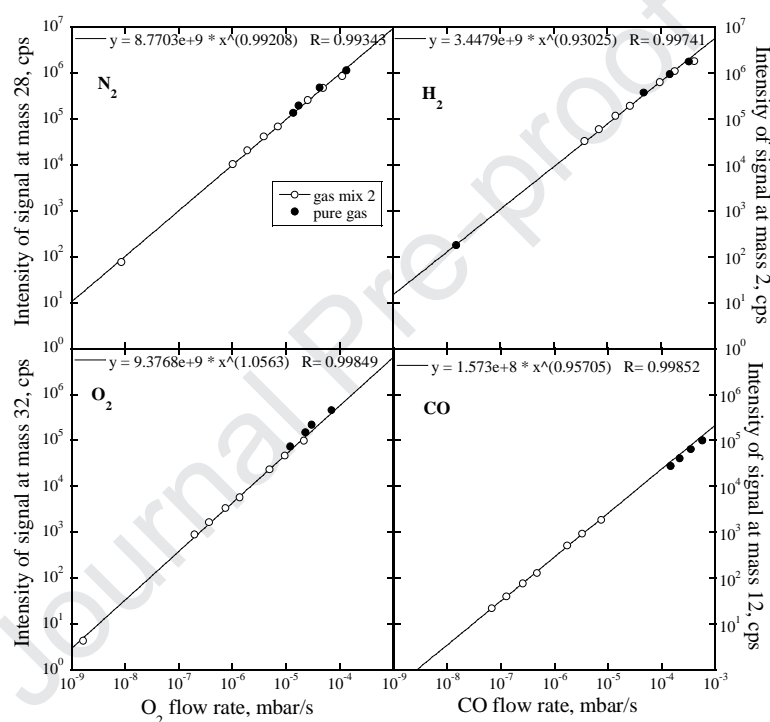
146   Figure 4. QMS sensitivity calibration.

147

148   However, the measured elemental ratios vary depending on flow rates (Fig. 5). The reason for this element

149   fractionation could be twofold: it can occur in the PZT valve during transition of gas to QMS and/or in the ion

150   source of QMS. Since the PZT valve works the same way as a capillary, element fractionation in it is

151   determined by the flow regime. With increasing flow rate/capillary diameter the heavy elements/isotopes show

152   enrichment compared to the lighter ones under a molecular flow regime. The sensitivity of QMS with respect to

153   different gas species is different due to variations in their ionisation potential. Additional fractionation can be a

154   result of mass discrimination in the ion source depending on pressure. These are complicated processes,

155   especially for chemically reactive gases, which can change the measured elemental ratios in the same direction

7

156   as it happens during mass fractionation in the PZT valve. As a result, it is difficult to distinguish between the

157   two processes.
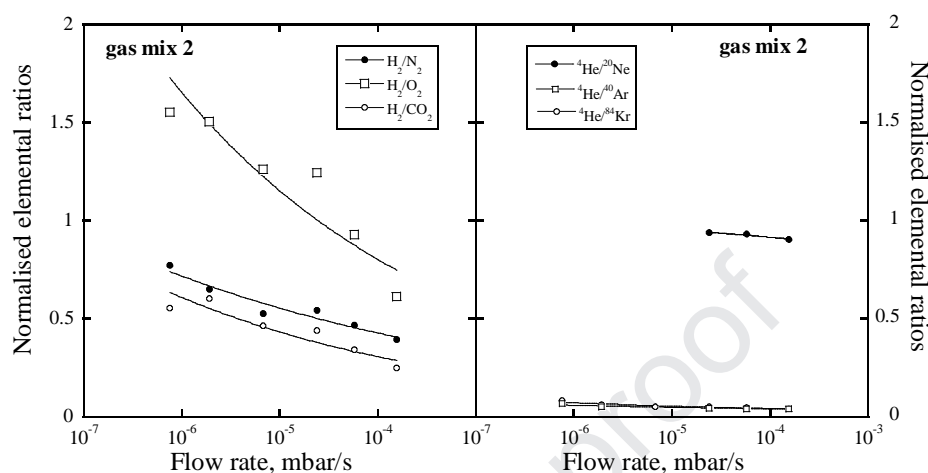
158

159   Figure 5. Element fractionation in QMS depending on flow rate.

160

161   The experimental data (Fig. 5) show that for chemically reactive gases the element ratios vary by a factor of

162   1.3-2 (depending on flow rate) to the direction expected under a molecular flow regime. On the other hand, for

163   chemically inert noble gases the variations are much smaller (almost negligible), though the relative differences

164   in masses for the former and the latter are similar. This suggests that the reason for fractionation is variations in

165   the relative sensitivity of QMS with respect to different chemically reactive gases depending on their pressure,

166   rather than fractionation in the PZT valve. The latter seems to provide mostly a viscous flow at 4-5 bar pressure

167   in the reference gas container that follows from almost no element fractionation for noble gases. In addition, as

168   it was mentioned above, if the variations of the elemental ratios (up to factor of 2) for chemically reactive gases

169   were caused by fractionation in the PZT valve, the data points on the calibration plots (Fig. 4) for pure gases and

170   gas mixtures would not make single calibration lines.

171   The use of pure gases for calibration enables the characterization of second order signals produced by some

172   molecular gases as a result of their dissociation in the QMS. The second order mass for N_2 is 14 ($^{14}N^+$), for CO

173   is 12 ($^{12}C^+$), for O_2 is 16 ($^{16}O^+$), CO_2 gives masses 28 ($^{12}C^{16}O^+$) and 16 ($^{16}O^+$) in nearly equal amounts and CH_4

174   gives mass 2 (H^+) (Fig. 6). The ratios between signals for the main and second order masses are in agreement

175   with observations made earlier (Hourlier, 2018), though the ratios depend on the QMS settings and flow rates.

176   Knowing the ratios between the main and second order signals for these gases allows us to calculate

177   contribution of different gas species when they are present in a mixture and therefore, may contribute towards

178   similar isobaric interferences, e.g. for N_2, CO and CO_2 at mass 28. When using a mixture of gases for calibration

179   in some cases it is better to use a second order signal instead of the main where interference is expected. For

180   instance, for CO calibration we used mass 12 instead of 28, which is mostly made of N_2 for our gas mixture, and

181   obtained a good calibration line including data for the gas mixture and pure CO (Fig. 4).

182
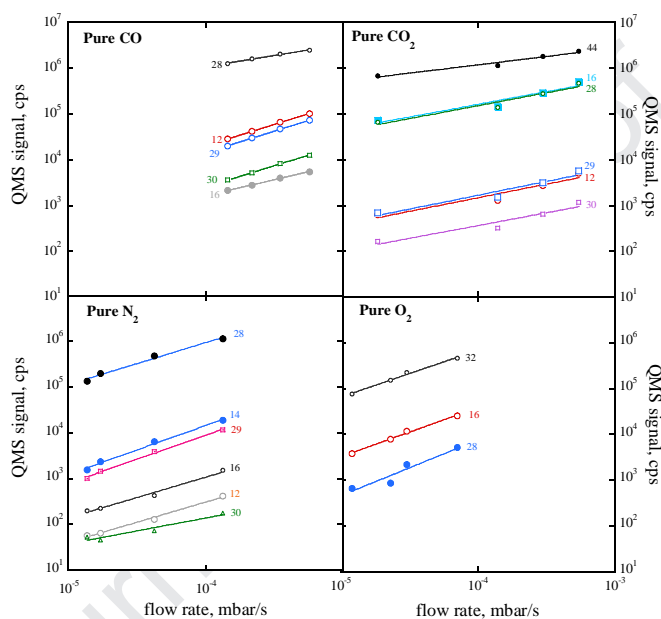
183
184   Figure 6. The main and the second order signals for pure gases.
185

186   It is important that calibration and sample analyses are made with the same QMS sensitivity. To control the

187   QMS sensitivity calibration should be repeated before and after each sample analysis.

188

189   3.3. *Testing the method with pure chemical compounds*

190

191   For this purpose we used solid samples such as $CaCO_3$ (NBS 18 standard), $CaC_2H_4*H_2O$, $NaHCO_3$ and PdO

192   (all from Fisher Scientific with more than 99% purity), which yield known (stoichiometric) amounts of gases

193   (CO, CO_2, O_2) during their thermal decomposition. Before and after each decomposition experiment we ran

194   calibration using pure gases, CO, CO_2, or O_2 and calculated amounts of the released gases using both

195   calibrations, which were in a good agreement with each other.

196   To calculate absolute amounts of the released gases we first translate corresponding signals in cps to cc/s

197   using calibration line. Since the experimental points are fitted with a power law in the form:

198

199   signal int. (cps) = a*(flow rate (cc/s))^b,

200

201   where a and b – the fitting parameters, the translation coefficient (k) is expressed as:

202

203   k=10$^{(\log(\text{signal int.})-\log(a))/b}$.

204

205   The amounts of gases released were calculated by integrating the release curve (in cc/s) over time as, for

206   example, shown in Figure 8. Obviously, the integration cannot be made analytically. Therefore, to determine the

207   area under the release curve we used "weighing method", consisting of printing the plot on a sheet of paper and

208   cutting it along the axes. Then, the weight of the whole plot area was determined using a precision balance.

209   Next, the area under the curve was cut and weighed. The amount of the released gas is then given by

210   □x*□y*(weight of the area under the curve/weight of the area of the whole plot), where □x and □y – are the

211   lengths of the plot along the axis in corresponding units. Verification of the method using a simple function that

212   can be integrated analytically, for instance y=x^2, gives an error about 1-2%.

213

214   3.3.1. Calcium carbonate

215   We analysed 5 different aliquots of pure CaCO$_3$. Thermal decomposition of CaCO$_3$ gives only CO$_2$ in the

216   temperature range 550-750 ^{o}C. In most of the analyses mass 44 was too high to measure since the signal

217   oversaturated the secondary electron multiplier and tended to level off at ~2x10^6 cps due to multiplier dead time

218   (~10^{-6} s). The problem with the saturation is caused by the necessity to find a compromise between QMS

219   sensitivity (in order to have good signals not only on the main but on the second order masses as well), the

220   sample size (to have a reasonable sample weighing error) and the reference gas flow rate (to avoid overpressure

221   in the QMS ion source). In this case, if possible, we used the second order signals at mass 12,16 or 28, which are

222   significantly smaller than that at mass 44 (see Fig. 6) with calibration at corresponding masses. Otherwise, if the

223   second order masses were too small to provide reasonably precise calculations, only a low limit of CO$_2$

224   concentrations can be estimated using the signal at the main mass, if the latter is saturated.

225   An example of the release pattern of CO$_2$ during thermal decomposition of CaCO$_3$ is show in Figure 7.

226   Maximum release is observed at 680°C in good agreement with known decomposition temperature of CaCO$_3$.

10

227   The signal at mass 44 is slightly cut off at maximum release due to the multiplier saturation effect. The mass 28

228   has an additional peak at 800°C; however, as there is no corresponding peak at mass 44, this is unlikely to be

229   CO_2, but could be CO or nitrogen.

230
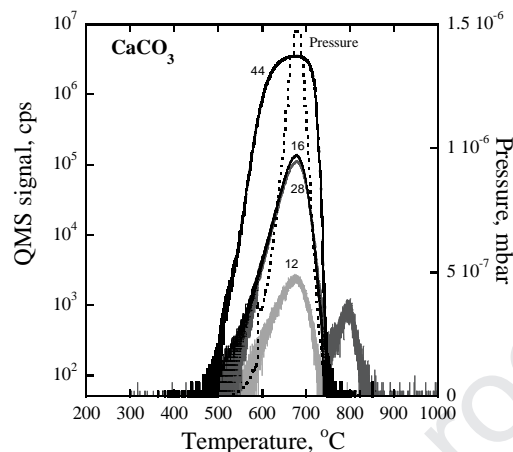
Figure 7. Kinetics of $CaCO_3$ decomposition during linear heating with 6°/min recorded at different masses.

231   Variations in the total pressure measured at QMS are also shown. Numbers next to curves indicate m/z.

232

233   In order to calculate the amount of CO_2 released we plotted the flow rate of CO_2 release (in cc/s) versus time

234   (Fig. 8). In this example we determined the area under the curve for mass 16 compared to the area of the whole

235   plot to be 0.170. The amount of CO_2 released is then determined as 5×10^{-5} cc/s* 4000 s* 0.170 = 0.330 cc.
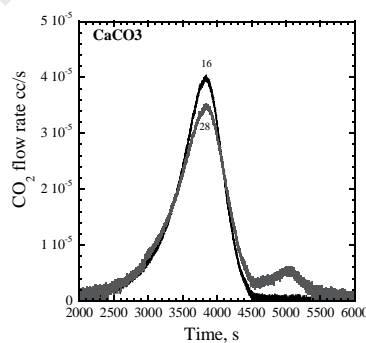
236

237   Figure 8. Release of CO_2 from $CaCO_3$ versus time at 6°/min for masses 16 and 28.

238   The kinetics of $CaCO_3$ decomposition depends on heating rate: at a higher heating rate the release peak is

239   broader with a maximum at a slightly higher temperature than at a lower heating rate (Fig. 9). But in general the

240   decomposition temperature, 700 ± 20°C, corresponds well to that known for $CaCO_3$.

11
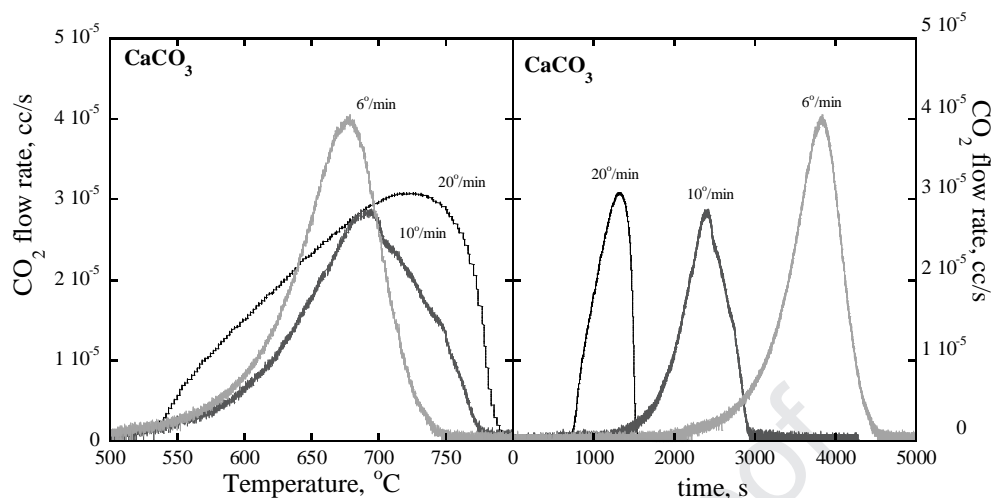
241

242   Figure 9. Decomposition of $CaCO_3$ as recorded at mass 16 at different heating rates.

243   The results of all analyses of $CaCO_3$ are listed in Table 2. There are no systematic differences between true

244   and calculated amounts depending on heating rate and masses used for calculations: the average deviation of all

245   calculated CO_2 amounts from the theoretical ones is -0.14±23% (1□).

246   Table 2. The theoretical and calculated amounts of CO_2 released during thermal decomposition of $CaCO_3$.

Sample mass, mg	Theoretical CO_2 content, cc	Heating rate, °/min	Calculated amounts of CO_2 for different masses			
			Mass 12	Mass 16	Mass 28	Mass 44
0.133	0.0298	6	0.0251	0.0328	0.0329	>0.0198
0.093	0.0208	20	n.a.	0.0165	0.0189	n.a.
0.109	0.0244	20	n.a.	0.0191	0.0172	n.a.
0.057	0.0128	20	0.0139	0.0158	0.0082	n.a.
0.074	0.0166	10	0.0202	0.0191	0.0245	0.0158

247

248   3.3.2. Calcium oxalate monohydrate

249   Thermal decomposition of $CaC_2O_4*H_2O$ produces water, carbon monoxide and carbon dioxide at 200, 500

250   and 600-700 °C respectively. Here we consider only release of CO and CO_2, since our system was not designed

251   for water analysis. In the major gas peak at 500 °C most of CO and ~25% of CO_2 are released. The higher

252   temperature gas release at 650 °C accounts for most of CO_2 and about 20% of CO (Fig. 10).
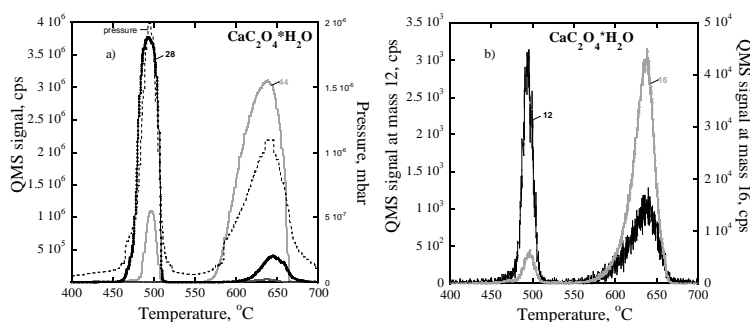
253

254 Figure 10. Thermal decomposition of $CaC_2O_4*H_2O$ at 12°/min heating rate. a) –the major peaks (masses 28 and

255 44) and the total pressure; b) – the second order peaks (masses 12 and 16).

256 Pure CO_2 and CO reference gases were used for calibration run before and after each sample. For calculations

257 of the amounts of CO_2 we used both the main and the second order signals, i.e. at mass 16 and 44 for CO_2, and

258 for CO – only mass 28, since signal at mass 12 has a significant contribution from CO_2. The results for calcium

259 oxalate monohydrate are summarised in the Table 3.

260 Table 3. The theoretical and calculated amounts of CO and CO_2 released during thermal decomposition of
261 $CaC_2O_3*H_2O$.

| Sample mass, mg	Theoretical CO_2 content, cc	Theoretical CO content, cc	Heating rate, ^{o}/min	Calculated amounts of CO_2 for different masses		
				Mass 28	Mass 16	Mass 44
0.063	0.0096	0.0096	20	>0.0062		0.0095
0.042	0.0064	0.0064	20	>0.0033	0.0074	>0.0049
0.047	0.0072	0.0072	20	>0.0040	0.0098	0.0063
0.067	0.00102	0.00103	12	0.0084	0.0121	0.0096
0.056	0.0086	0.0086	12	0.0081		0.0088

262

263 The average value and standard deviation of the calculated values from the theoretical one is 3±17%,

264 basically similar to the result obtained for $CaCO_3$.

265

266 3.3.3. Palladium oxide

267

268   Thermal decomposition of PdO yields 13.1 wt % oxygen at about 650 ^{o}C (Fig.11). The second order signal is

269   observed at mass 16. The main signal at mass 32 was in all measurements (3 samples) too high to provide

270   accurate calculations.
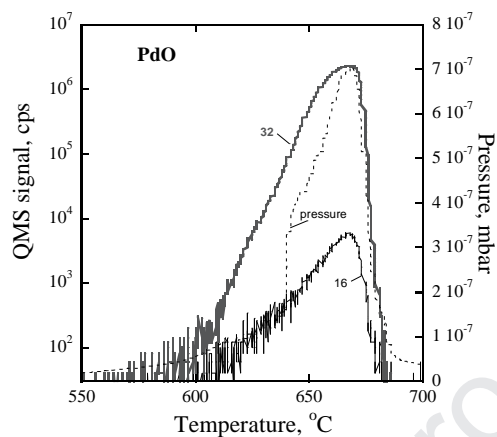
271

272   Figure 11. Thermal decomposition of PdO at 12°/min heating rate. Numbers next to curves indicate m/z.

273   The deviations of the calculated amounts of O_2 from the theoretical ones (Table 4) in the samples analysed

274   show similar scatter as was observed for other compounds (see sections 3.3.1 and 3.3.2.).

275   Table 4. The theoretical and calculated amounts of O_2 released during thermal decomposition of PdO.

Sample mass, mg	Theoretical O_2 content, cc	Heating rate, ^{o}/min	Calculated amounts of O_2 for different masses, cc	
			Mass 16	Mass 32
0.077	0.0071	20	0.0086	>0.0040
0.196	0.018	12	0.025	>0.069
0.106	0.0097	12	0.0082	>0.051

276

277   3.3.4. Sodium bicarbonate

278   Thermal decomposition of $NaHCO_3$ occurs at about 170°C with formation of H_2O and CO_2 (Fig. 12).

279

14
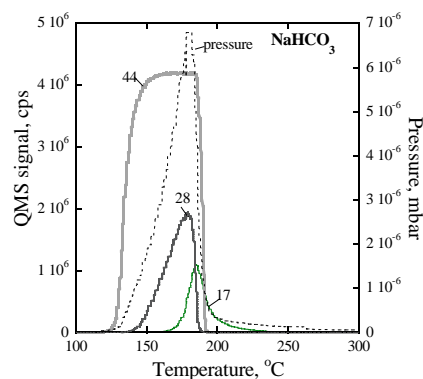
280   Figure 12. Thermal decomposition of $NaHCO_3$ at 12°/min heating rate. Numbers next to curves indicate m/z.

281   The signals at masses 44 and 18 were saturated, therefore, to quantify the amounts of CO_2 and water we used

282   the second order signal at mass 28 and 17 respectively. It gives 0.026 cc of CO_2 versus 0.022 cc expected from

283   the 0.164 mg sample aliquot used in the decomposition experiment. The difference is within the same range of

284   uncertainty as observed for other decomposition experiments (see above).

285   The clear release peak of H_2O from the sample suggests that water can be registered in spite of its

286   condensation in the pipes between the extraction furnace and QMS. This result is used to calibrate the QMS for

287   water. For that we calculated the integral of mass 17 signal over time that consists of 1.24×10^8 cps, which

288   corresponds to the 1.75×10^{-5} g of water in the sodium bicarbonate sample analysed. Thus, we found the QMS

289   sensitivity factor for water to be 1.41×10^{-13} g/cps, which we used for evaluation of water content in the meteorite

290   samples (see section 5) suggesting that condensation process for the reference and meteorite samples occurs in a

291   similar way.

292

293   4. Analysis of errors associated with QMS calibration

294   The plot in Figure 13 summarises the result for all chemical compounds analysed. As can be seen, the

295   distribution of the relative deviations of the measured amounts from those calculated for the compounds is

296   almost symmetrical with median value close to zero pointing to a good accuracy of the measurements. The

297   standard deviation of the distribution is 22%.
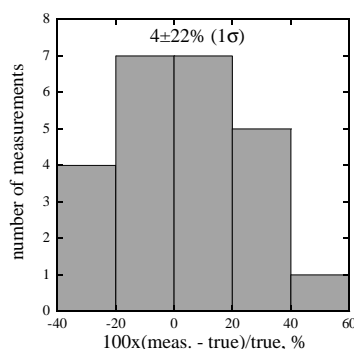
299   Figure 13. Distribution of the relative deviations between measured and true concentrations of gases for

300   chemical compounds analysed.

301   Since the flow rate calibration curves represent a power function and the sample gas flow rate is calculated

302   in the form of $10^{(\log(x)-\log(a))/b}$, where x is the measured sample signal and a and b are calibration curve fitting

15

303   parameters, the errors of a and b are very critical for the error of the flow rate. For a typical calibration curve

304   shown in Figure 14a the errors for a and b can be found if x and y are replaced by their logarithms (Fig. 14b).

305   The calibration line is transformed into a straight line for which errors of intercept and slope can be calculated

306   using square root method. For the given example the expression for flow rate is $x=10^{(log(y)-}$

307     $^{(13.973\pm0.406))/(2.5883\pm0.0960)}$, where y is the signal at mass 12 measured during decomposition of the $CaCO_3$ sample.

308   We used the error propagation calculator

309   (www.colby.edu/chemistry/PChem/scripts/error.html?ModPagespeed=off) to calculate error of the above

310   expression, which consists ~45% of the x (flow rate) value. Similar relative error is obtained for the amount of

311   CO_2 released after integration of the release curve (Fig. 14c). The results presented in the tables 2-4 show

312   somewhat lower errors than estimated mostly because we used several calculations for the same sample that

313   should reduce the uncertainty. In order to reduce the error for the amount of gas to ~15% the errors for the slope

314   and intercept of the calibration line should be reduced from actual 3-4% to ~1%. This seems to be achievable if

315   the major signals are measured on Faraday cap and the minor – on multiplier. Our model of QMS does not

316   however allow this.
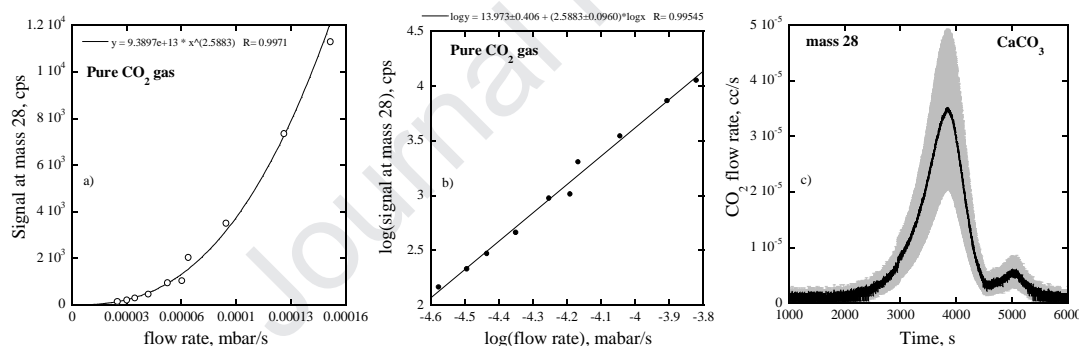
317

318   Figure 14. Error propagation for the calculated amounts of the released CO_2. a) – calibration curve in linear

319   scale, b) – calibration curve in logarithmic scale with errors, c) – release of CO_2 with error bars (shadow area).

320

321   5. Analyses of the standard meteorite samples Murchison and Allende

322   As part of ESA's PROSPECT lunar exploration activity, two reference samples of Murchison (CM2) and

323   Allende (CV3) meteorites have been developed as standards for volatile species investigations (Mortimer et al.,

324   2017). Isotopic compositions and concentrations of C, N and some noble gases have been analysed in these two

325   samples using different methods. Below we explain how the EGA of the samples can be explained and

326   quantified on the basis of the calibration procedures discussed above.
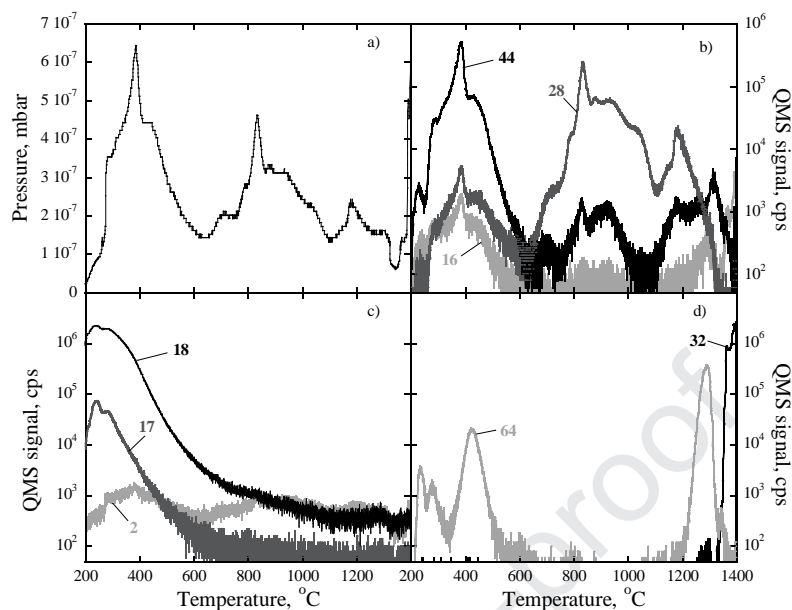
327

328   Figure 15. Release patterns of different gas species (b-d) and pressure variations (a) during EGA of the Allende

329   meteorite standard with heating rate 12 ^{o}C/min. Numbers next to curves indicate m/z.

330   5.1. Allende

331   A 3.29 mg sample was used for the QEGA. As can be seen from Figure 15a, there are three major peaks of

332   pressure which coincide with the peaks of QMS signals at masses 44 and 28 (Fig 15b). The first low

333   temperature peak is represented mostly by mass 44 with much smaller but similar shaped peaks at masses 16

334   and 28. This is a good indication that the low-temperature peak is made predominantly of CO_2. The major

335   contribution for the middle- and high-temperature peaks is from mass 28. At the same time, the peaks at mass 44

336   and 16 are significantly lower in this temperature range. This represents clear indication that the middle- and

337   high-temperature peaks correspond to release of CO. If there is a contribution from nitrogen on these peaks, it

338   must be very low, since no signal at mass 14 is observed.

339   Using calibration with pure CO_2 gas we calculated the amounts of C released at low and high temperature

340   range. For the low temperature peak of CO_2 (200-600 ^{o}C) we used the signal at mass 44 and obtained

341   0.14±0.04% of the total C in the sample. For the high-temperature release of CO the signal at mass 28 has been

342   used that gives 0.20±0.05% of the total C in the sample. So, the total calculated C concentration in the sample is

343   0.34±0.07% vs. 0.4±0.1% obtained by another independent methods (Mortimer et al., 2017). Taking into

344   account all associated uncertainties with the QEGA measurements and data reduction (~30%), there is a

345   reasonable agreement between the two methods.

346   Release of SO_2 is clearly indicated by signal at mass 64 (Fig. 15d). There are two low- and high-

347   temperature releases of the gas associated with decomposition of different sulphur compounds such as troilite

348   and pentlandite and oxidation of sulphur as a result of chemical reactions with oxygen containing minerals.

349   Notably the high-temperature release of SO_2 does not coincide with the release of pure oxygen at the very high

350   temperature. The latter appears to be a result of decomposition of SiO_2 vapours produced by the hot quartz of

351   the extraction furnace sample tube at T >1300 ^{o}C that coincides with significant increase of pressure. Pt foil

352   used to wrap the samples acted as a catalyst for the process. Apparently, this oxygen does not play an important

353   role in the production of SO_2. Hydrogen release is broad (Fig 15c) and seems to be associated mainly with

354   decomposition of organic compounds. Calculation of the hydrogen absolute amount using calibration with gas

355   mixture 2, containing 57 vol. % of hydrogen (Table 1) gives 0.01 wt. % H, which is close to the values

356   determined by other methods, 0.006 wt. % (Kerridge, 1985; Alexander et al., 2007).

357   Finally, there is a clear release of water mostly at low temperature (Fig. 15c) recorded simultaneously at

358   masses 18 and 17 (OH). Both peaks are broad with long tails suggesting that water had condensed in the pipes

359   between the extraction furnace and QMS. We, however, believe that the low temperature release pattern of

360   water is basically not far from its true release in spite of water condensation on cold parts of the vacuum system.

361   This conclusion is based on the result of analyses of sodium bicarbonate which we used to evaluate the water

362   content in the meteorite samples. With the QMS sensitivity factor obtained for water (see section 3.3.4) we

363   calculated the total water content in the Allende standard using mass 17 to be 0.11 wt. %, which is in the range

364   obtained for this meteorite earlier, 0.11-0.16 wt. % (Robert and Merlivat, 1977) and 0.24 wt. % (Eiler and

365   Kitchen, 2004).

366

367   5.2. Murchison

368   2.02 mg of the Murchison sample was also analysed by QEGA. The pressure variations show basically a

369   single broad peak with a spike at 690 ^{o}C (Fig.16a). The release of most of major gases follow generally the same

370   pattern. The signal at masses 44 and 28 are mostly overlapping, though in detail, considering signals at masses

371   12 and 16, one can conclude that CO_2 is dominating in the temperature range 200-500 ^{o}C, while CO in the range

372   500-1000 ^{o}C (Fig. 16b). For both gases there is a spike at 690 ^{o}C. In a sense this is similar to what was observed

373   for CO_2 and CO releases from Allende, though without such an extensive overlap. It is considered likely that

374 release of these gases occurs due to chemical reactions between carbon and oxygen containing phases. The spike

375 is obviously an indication of changing in the rate of the reactions A small signal at mass 16 at very high (>1200

376 $^{\circ}$C) temperature not supported either by a signal at mass 28 or at mass 44, is probably due to methane.

377   Release of SO_2 is bimodal (Fig. 16d) and observed in the similar manner to that for Allende temperature

378 range, indicating the presence of a similar sulphur containing mineral(s) in both meteorites. A peak of pure

379 oxygen is also observed at very high temperature similar to that in case of Allende and has the same nature

380 associated with SiO_2 vapours from the quartz extraction tube. Water is released mostly at relatively low

381 temperature (Fig. 16c), but at higher concentration than for Allende. In general, the volatiles content in

382 Murchison is significantly higher than in Allende, which can be seen in the signal intensities as well as in the

383 total pressure recorded, especially considering that the sample size of the latter was larger by a factor of 1.5

384 compared to the former. This difference seems to be in line with the metamorphic grade of the meteorites (CM2

385 and CV3), consistent with the loss of volatiles during parent body metamorphism.
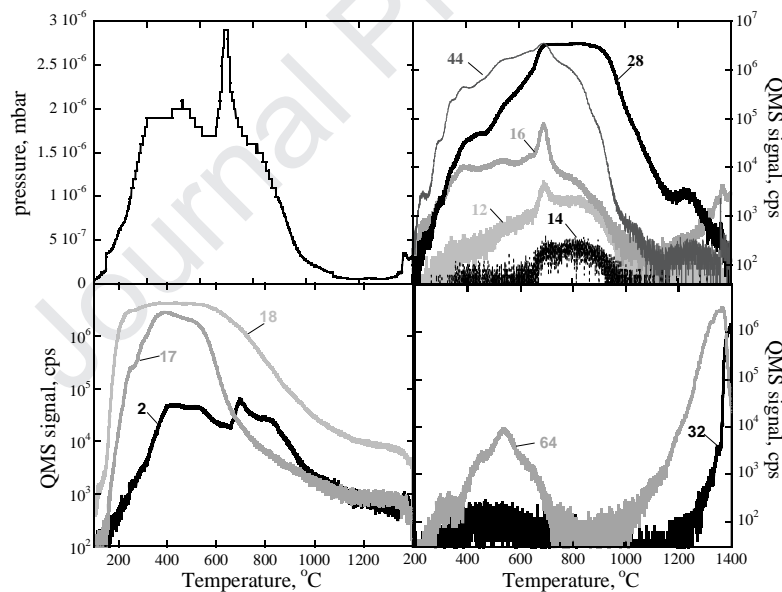
386

387   Figure 16. Release patterns of different gas species (b-d) and pressure variations (a) during EGA of the

388   Murchison meteorite standard with heating rate 12 $^{\circ}$C/min. Numbers next to curves indicate m/z.

389   Calculation of C concentration in the sample using signal at mass 16 as the measure of CO_2 amount and

390 at mass 12 for CO amount gave the total amount of C higher than expected: 5.4% vs. ~2% (Mortimer et al.,

391 2017). Similar discrepancy is obtained for water content: 20% vs. ~8% (Robert and Epstein, 1982; Jarosewich,

392 1971). The reason for such differences is currently not fully understood. This may be because mass 12

393 represents not only CO but has some contribution from CO_2. This could also be due to a contribution of other

394 species such as methane on mass 16. The other explanations could be that during analysis of the sample the

395 pressure in the QMS was quite high and therefore the overall conditions (in particular element fractionation in

396 the QMS) were different from those that have been during calibration. The difference in the pressure conditions

397 can also affect condensation of water and, therefore, it was different from that for the reference sample. All

398 these possibilities will be investigated in our further development of the method. For hydrogen, which, in

399 contrast to Allende, is released together with other major gases, we obtained a reasonable concentration, 0.06

400 wt. %, which is close to the range for this meteorite: ~0.1 (Alexander et al., 2010) and 0.074 wt. % (Kerridge,

401 1985). Close to the expected concentration we also obtained for nitrogen using signal at mass 14: 0.07 % vs.

402 0.08% (Mortimer et al., 2017).

403

404 6. Concluding remarks

405   We consider this study as a first step towards quantitative EGA of extra-terrestrial samples. A method of

406 QMS calibration with reference gases (pure or gas mixture) with known flow rate has been developed along

407 with flow rate calibration procedures. Testing the method with chemical compounds that can be thermally

408 decomposed into gaseous components with well-known yields demonstrated accuracy though not particularly

409 precise results. Future work will focus on improving the precision. For example, for major masses such as 2, 18,

410 28, and 44 could be measured using Faraday cups, while the minor masses could be registered using electron

411 multipliers. In such cases, the multiplier saturation effect can be avoided and the signal to noise ratio for minor

412 masses can be increased using a higher multiplier voltage. Along with the calibration we have developed an

413 approach for more reliable identification of gas species in the multicomponent mixtures based on the analysis of

414 mass spectra of the first and second order signals of certain gases. The application of the developed EGA to the

415 meteorite standard samples of Allende and Murchison in most cases yielded reasonable results. However, the

416 method requires further development and improvement, in particular for water measurements. These would

417 benefit from a vacuum system that can be fully heated to ~120 °C to reduce condensation of water on internal

418 surfaces and thus increase the efficiency of transfer to the QMS. A similar system has already been built in our

419 laboratories for different purposes and provision for such heating has been made in the ProSPA instrument

420 which will attempt QEGA *in situ* on the Moon within the Luna-27 mission.

421 Acknowledgements

425

426   References:

427   Alexander C. M. O'D., et al. (2007) The origin and evolution of chondrites recorded in the elemental and

428   isotopic compositions of their macromolecular organic matter. *Geochim. Cosmochim. Acta* **71**, 4380-4403.

429   Alexander C. M. O'D., et al. (2010). Deuterium enrichments in chondritic macromolecular material –

430   Implications for the origin and evolution of organics, water and asteroids. *Geochim. Cosmochim. Acta* **74**,

431   4417-4437.

432   Anand, M., Crawford, I. A., Balat-Pichelin, M., Abanades, S., van Westrenen, W., Péraudeau, G., Jaumann, R.,

433   Seboldt, W. (2012). A brief review of chemical and mineralogical resources on the Moon and likely initial in

434   situ resource utilization (ISRU) applications. *Planet Space Sci* **74** (1), 42-48

435   Barber S. J. et al. (2018) ProSPA: Analysis of Lunar Polar Volatiles and ISRU Demonstration on the Moon.

436   49th Lunar and Planetary Science Conference, abstract # 2172.

437   Chamberlin R. T. (1909) The gases in Rocks. *The Journal of Geology* **17**, 534-568.

438   Eiler J. M, and Kitchen N. (2004) Hydrogen isotope evidence for the origin of the carbonaceous chondrites.

439   *Geochim. Cosmochim. Acta* **68**, 1395-1411.

440   Gibson E. K. and. Johnson S. M (1971) Thermal analysis-inorganic gas release studies of lunar samples. *Proc.*

441   *Second Lunar and Planet. Sci. Conf.* **2**, 1351-1366.

442   Gibson E. K. and Moore G. W. (1972) Inorganic gas release and thermal analysis study of Apollo 14 and 15

443   soils. *Proc. Third Lunar and Planet. Sci. Conf.* **2**, 2029-2040.

444   Hourlier D. (2018) Thermal decomposition of calcium oxalate: beyond appearances. *J. Thermal Analysis and*

445   *Calorimetry*, https://doi.org/10.1007/s10973-018-7888-1.

446   Jarosewich E. (1971). Chemical analysis of the Murchison meteorite. *Meteoritics* **6**, 49-52.

447   Kerridge J. F. (1985) Carbon, hydrogen and nitrogen in carbonaceous chondrites: Abundances and isotopic

448   composition in bulk samples. *Geochim. Cosmochim. Acta* **49**, 1707-1714.

449   Maciejewski M. and Baiker A. (1997) Quantitative calibration of mass spectrometric signals measured in

450   coupled RA_MS system. *Thermochimica Acta* **295**, 95-105.

451   Ming D. W. et al. (2014) Volatile and organic composition of sedimentary rocks in Yellowknife Bay, Gale

452   crater, Mars. *Science* **343**, 1245267.

453   Mortimer J., Anand M., Verchovsky A. B., Nicoara S., Greenwood R. C., Gibson J., Franchi I. A., Ahmed F.,

454   Strekopytov S., and Carpenter J. (2017). Preparing and Characterizing Carbonaceous Chondrite Standards for

455   Verification of ESA'S 'Prospect' Package. In: 48th Lunar and Planetary Science Conference, 20-24 Mar 2017,

456   The Woodlands, Houston, Texas, abstract # 2113.

457   Risoluti R. and Materazzi S. (2018) Mass spectrometry for evolved gas analysis: An update. *Applied*

458   *Spectroscopy Reviews*, https://doi.org/10.1080/05704928.2018.1452252.

459   Robert F. and Merlivat L. (1977) Water and deuterium content in eight chondrites. *Meteoritics* **12**, 349-354.

460   Sheridan S, Jarvis M. and Morgan G. H. (2010) Miniature valve for helium flow control. The Open University,

461   Patent PCT/GB2009/002584.

462   Verchovsky A. B. (2017) Origin of isotopically light nitrogen in meteorites. *Geochemistry International* **55**,

463   969-983.

464   Xia H. and Wei K. (2015) Equivalent characteristic spectrum analysis in TG-MS system. *Thermochimica Acta*

465   **602**, 15-21.

466   Xiao M. at al. (2019) Gas release systematics of mineral-hosted fluid inclusions during stepwise crushing,

467   implications for $^{40}Ar/^{39}Ar$ geochronology of hydrothermal fluids. *Geochim. Cosmichim. Acta* **251**, 36-55.

The paper describes a quantitative evolve gas analysis with application to two meteorite samples. The method is based on calibration of the quadrupole mass spectrometer sensitivity with respect to different gases using flows of pure gases and gas mixtures as references which flow rates were determined by an independent method. The method was verified by analyses of pure chemical compounds decomposing into simple gases upon heating.

AUTHOR DECLARATION

We wish to draw the attention of the Editor to the following facts which may be considered as potential conflicts of interest:

Drs Sheridan and Morgan are employees of The Open University and are founders/directors of Applied Science & Technology Solutions Ltd that has a Manufacturing License Agreement with The Open University to commercialise the patented PZT valve. They are both named inventors on the OU patent. The valves used in this study were manufactured at The Open University.

We confirm that the manuscript has been read and approved by all named authors and that there are no other persons who satisfied the criteria for authorship but are not listed. We further confirm that the order of authors listed in the manuscript has been approved by all of us.

We confirm that we have given due consideration to the protection of intellectual property associated with this work and that there are no impediments to publication, including the timing of publication, with respect to intellectual property. In so doing we confirm that we have followed the regulations of our institutions concerning intellectual property.

We understand that the Corresponding Author is the sole contact for the Editorial process (including Editorial Manager and direct communications with the office). He is responsible for communicating with the other authors about progress, submissions of revisions and final approval of proofs. We confirm that we have provided a current, correct email address which is accessible by the Corresponding Author and which has been configured to accept email from (sasha.verchovsky@open.ac.uk).

Signed by all authors as follows:

Sasha Verchovsky.. Date: 23.05.19

Mahesh Anand.. Date: 24.05.19

Simeon Barber.. Date: 23 May 2019

Simon Sheridan.. Date: 26/05/19

Geraint Morgan.. Date: 23/5/19